Available online at www.sciencedirect.com
ScienceDirect
Journal of Nuclear Materials 363–365 (2007) 680–685
journal of nuclear materials
www.elsevier.com/locate/jnucmat

Characterization of transport in the stochastic edge layer of TEXTOR by analysis of the radial and poloidal distribution of electron density and temperature

O. Schmitz *, D. Harting, S.S. Abdullaev, S. Brezinsek, K.H. Finken, H. Frerichs, M. Jakubowski, M. Lehnen, X. Loozen, Ph. Mertens, D. Reiter, U. Samm, B. Schweer, G. Sergienko, M.Z. Tokar, B. Unterberg, R.C. Wolf and the TEXTOR team

Institut für Plasmaphysik, Forschungszentrum Jülich, Association EURATOM-FZJ, Trilateral Euregio Cluster, Germany

Abstract

At TEXTOR the dynamic ergodic divertor (DED) induces a stochastic edge layer by a resonant magnetic perturbation to control heat and particle exhaust. In this paper the characterization of its generic transport properties is described. The radial and poloidal distribution of electron density and temperature is analyzed accompanied by observations of the particle flux to the DED target. These experimental results are compared to the calculated magnetic topology and to results from EMC3/EIRENE modeling. Thereby, the existence of two poloidally separated transport domains is demonstrated: laminar flux tubes are dominated by parallel transport to the DED target – they act analogous to a classical scrape-off layer. In contrast, the adjacent ergodic domains show stochastic transport characteristics with enhanced radial transport.

PACS: 52.25.Fi; 52.55.Fa; 51.60.+a

Keywords: Ergodic divertor; Edge transport; Stochastic boundary; Edge modelling; TEXTOR–DED

1. Introduction

The application of a stochastic edge layer promises an improvement of particle and heat exhaust in present-day magnetic confinement schemes: in helical devices and stellarators [1] stochastic layers intrinsically exist and are utilized in exhaust concepts such as the helical divertor [2] or the island divertor [3]. In tokamaks, the stochastic behavior of the magnetic field lines is vital to improve the exhaust characteristics of the poloidal divertor: an improvement of the impurity screening, an optimized particle recycling and the mitigation of the peak heat loads caused by edge localized modes [4] are key subjects for possible improvements through a stochastic edge layer [5]. The dynamic ergodic

* Corresponding author. Fax: +49 2461 612660.
E-mail address: o.schmitz@fz-juelich.de (O. Schmitz).
URL: http://www.fz-juelich.de/ipp (O. Schmitz).

0022-3115/$ - see front matter
doi:10.1016/j.jnucmat.2007.01.067

divertor (DED) at the TEXTOR tokamak is a flexible setup to create an external magnetic perturbation with different poloidal/toroidal base mode numbers of $m/n = 3/1$, 6/2 and 12/4 in static or dynamic (1–10 kHz) operation [6]. Detailed calculations of the induced magnetic topology by simplectic mapping methods [7] showed that it consists of two kinds of field lines with rather different transport properties expected: *laminar field lines* [5,6,8] – with a short connection length – are assumed to impact on the edge through a dominating parallel transport to the wall. Therefore, they will act similarly to those in the scrape-off layer (SOL) of poloidal divertor or limiter machines. The adjacent longer field lines – called *ergodic field lines* – have a stochastic character which causes enhanced field line diffusion and thus presumably an increased radial transport of particles and energy [8,9]. These topological features emerged to be similar to those in the stochastic edge layers of other experiments as Tore Supra [10] or the large helical device [2] for example. However, the advanced tools developed to analyze the magnetic topology of the DED-induced stochastic edge layer [6] give detailed topological information in radial and poloidal direction. This allows direct comparisons with experimental results: in this paper, the measured radial and poloidal distribution of electron density n_e and temperature T_e is compared to the calculated magnetic topology in order to characterize the generic transport properties. These investigations are supported by a first modeling of the plasma structure with the EMC3/EIRENE code.

2. Experimental setup

The poloidal and radial distributions of n_e and T_e were measured by means of beam emission spectroscopy (BES) on thermal helium [11]. Two atomic beam systems were applied: one at the low field side (LFS) (toroidal angle $\varphi = 270°$, poloidal angle $\vartheta = 5°$, slightly below midplane) and the other one at the high field side (HFS) ($\varphi = 180°$, $\vartheta = 185°$, slightly above midplane) in front of the DED target tiles. These diagnostics have a spatial resolution of 1.2 mm and radial $n_e(r)$ and $T_e(r)$ profiles of 4–8 cm extent can be typically obtained. These results were supported by measurements with CCD cameras equipped with H_α interference filters ($\lambda = 656.3$ nm, $\Delta\lambda = 5$ nm). They observe perpendicularly to the DED target and the collected light intensity of the $H_\alpha(\vartheta, \varphi, t)$ emission is therefore used as a measure for the particle flux $\Gamma(\vartheta, \varphi, t)$ to the DED target.

For the discharges under discussion, the DED was operated in $m/n = 12/4$ base mode configuration, characterized by a shallow penetration of the perturbation field and small scaled magnetic structures [6]. The poloidal direction of the stochastic edge layer is inspected by a sweep of the DED current distribution. This relocates the magnetic topology poloidally by $\Delta\vartheta = 10°$ at LFS and $\Delta\vartheta = 4.5°$ at HFS without changing the topological structure itself.

The results presented in this paper were deduced from two exemplary discharges #96620 and #95924. The characteristic parameters are: effective DED current I_{DED}=7.5 kA, plasma centre $R_0 = 1.73$ m, minor radius $a = 45.7$ m, toroidal magnetic field $B_t = 1.9$ T, plasma current $I_P = 400$ kA, edge safety factor $q_a = 3.2$ and heating power $P_H = 1200$ kW.

3. Plasma structure and generic transport properties

We start the discussion of the experimental findings in front of the DED target at the HFS and continue with a more detailed analysis at the LFS. As discussed in [12], the particle flux $\Gamma(\vartheta, t)$ to the DED target is redistributed with increasing perturbation into four pairs of strike zones distinguished by regions of vanishing particle flux. Fig. 1(a) shows the time evolution of one pair of these strike zones during a sweep of the DED currents. The particle flux follows the triangular shaped waveform of the current modulation and the excursion of the strike zones fits to the calculated value of $\Delta\vartheta = 4.5°$ for the HFS. Fig. 1(b) depicts the electron pressure $p_e(r, t)$ in front of the DED target for the same discharge: $p_e(r, t)$ is reduced during the whole current sweep and a modulation of $p_e(r, t)$ does not occur. This can be explained by taking into account the location of the diagnostic inside the induced structure: as visualized by the dashed line in Fig. 1(a), the helium beam diagnostic at HFS is located inside the region without a significant particle flux. Comparisons with the magnetic topology show that the magnetic field lines in this region reconnect to the target with very short connection lengths ($L_c \lesssim 5$ m) and without relevant radial excursion into the plasma edge layer. This region is therefore classified as the private flux region (PFR) of the ergodic divertor structure induced by the DED. The isobar lines in Fig. 1(b) are displaced radially

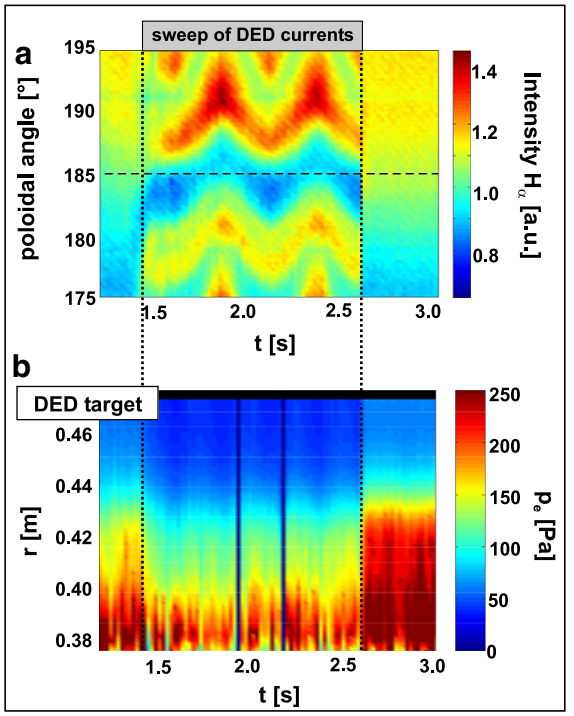

Fig. 1. Change of the plasma edge structure during a strike point sweep (TEXTOR discharge #96620): (a) shows the particle flux on the DED target in the vicinity of the Helium beam diagnostic at HFS (dashed line). In (b) the time dependence of the radial distribution of electron pressure $p_e(r,t)$ in front of the DED target is visualized.

inward by 2–3 cm which fits to the calculated radial extension of the PFR. The strong drop of $p_e(r,t)$ and the vanishing particle flux in this region proves that the PFR is efficiently separated from the adjacent finger structures described in [7].

To analyze the data obtained at the LFS, the time evolutions of $n_e(r,t)$ and $T_e(r,t)$ were converted to a radial–poloidal distribution $n_e(\vartheta,r)$ and $T_e(\vartheta,r)$ (TEXTOR #95924). During one sweep period, the magnetic topology is relocated in front of the atomic beam diagnostic such that the observation volume is continuously moved from $\Delta\vartheta = 5°$ to $\Delta\vartheta = 15°$ for the first half period and back for the second. This poloidal angle is used as y-axis in Fig. 2(a) and x-axis in Fig. 2(b), respectively.

Fig. 2(a) shows the comparison of $n_e(\vartheta,r)$ and $T_e(\vartheta,r)$ to the connection length $L_c(\vartheta,r)$ as the field line length from target to target in poloidal turns (p.t.): both n_e and T_e are reduced at the position of field lines with short $L_c = 1$–2 p.t. – the so called *laminar field lines*. In the adjoining regions filled by field lines with long connection length ($L_c \geqslant 3$ p.t.) n_e and T_e are up to a factor of 2 higher. These field lines are therefore classified as *ergodic field lines*. This opposite behavior of the electron parameters in both topological domains is emphasized in Fig. 2(b). Here the direct comparison of poloidal cuts of electron pressure $p_e(\vartheta)$ and $L_c(\vartheta)$ at four radial positions is shown. It becomes clear that, in contrast to the laminar region, the adjacent long connection length regions yield to higher values of p_e. These experimental findings prove that the plasma structure in the stochastic edge is heavily influenced by the magnetic topology in terms of L_c and they allow to characterize the generic transport properties in the two very different domains.

The *laminar field lines* connect within a distance of about 15–45 m directly into the strike zone on the DED target tiles. On these short distances they do

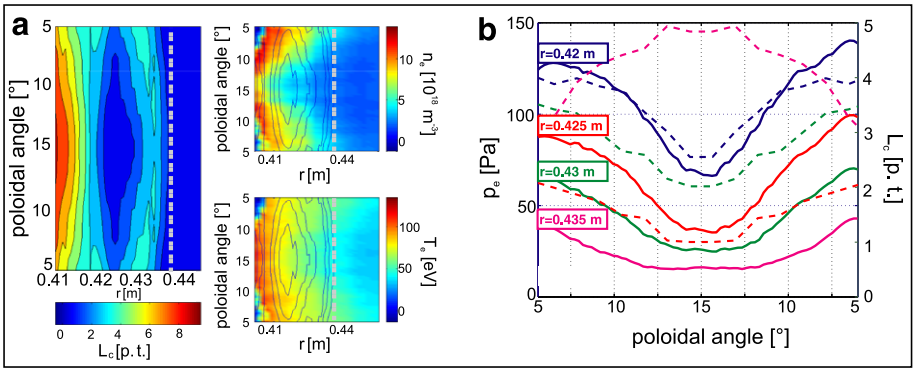

Fig. 2. Correlation of the plasma structure with the magnetic topology: (a) shows the connection length pattern $L_c(\vartheta,r)$ in poloidal turns (left figure) in comparison to $n_e(\vartheta,r)$ (upper right figure) and $T_e(\vartheta,r)$ (lower right figure). The contours of $L_c(\vartheta,r)$ are superimposed and the position of the LCFS without perturbation is marked as dashed line. (b) Shows poloidal profiles of the electron pressure $p_e(\vartheta)$ at different radii (solid lines, left axis) and the $L_c(\vartheta)$ profiles at the same radial positions (dashed lines, right axis, same colours sketch same radial positions).

not deviate from each other but stay in a helical flux tube from their start point to their end point on the DED target [6,8]. These so-called *laminar flux tubes* have a large radial and poloidal extension: for the discharge discussed, an extension of 2–3 cm in radial and about 10 cm in poloidal direction was deduced from the calculated magnetic topology.

To answer the question whether laminar flux tubes of this size can extract particles and energy from the plasma edge by parallel transport to the wall, this size is compared to the e-folding lengths λ_n and λ_T of the $n_e(r)$ and $T_e(r)$ profiles. We refer to these quantities as a typical transport length scale in the vicinity of field lines with short connection to the wall, i.e. the scrape off layer in limiter or poloidal divertor machines [13]. Their values were deduced in the unperturbed phase of the discharge and amount to $\lambda_n = 21$ mm and $\lambda_T = 51$ mm.

These values indicate a higher diffusive transport for the energy than for the particles. This explains the observed difference in the quantitative reduction of n_e and T_e: the electron density n_e is reduced by a factor of 2 whereas the electron temperature T_e is reduced only by about 25%. For particles, this means that the parallel convective transport to the wall can compete with the diffusive radial transport: the extension of the flux tube is large enough to efficiently extract particles from its volume. For energy, the diffusive radial transport is higher, therefore the decay of T_e within the radial extension of the flux tube is weaker. The main impact on the temperature distribution is caused most likely by the convective losses due to the particle flow in the laminar flux tubes.

Contrary to this, n_e and T_e are higher in the adjacent *ergodic regions* for two reasons: first, the field lines make in between each toroidal transit radial excursions of up to 2 cm inward. By this means they connect the region next to the laminar flux tubes with hotter regions of higher density at smaller radius (located at the last undestroyed island chains) [14]. This leads to an efficient filling of these ergodic regions by parallel transport. However, these field lines do not connect directly to the wall but have $L_c > 90$ m. This is much higher than typical values of the Kolmogorov length L_K ($L_K = 30$ m at $r = 0.40$ m for the present discharge) as a measure for the decorrelation of neighboring field lines [6,7]. The ergodic field lines are therefore characterized by a enhanced field line diffusion (local field line diffusion coefficient [6] $D_{FL} \simeq 3 \times 10^{-6}$ m^2/m) and thus by an effectively increased radial transport. Both effects together lead to a filling of the ergodic regions surrounding the laminar flux tubes. They channel the incoming radial particle and heat fluxes towards the DED target. The parallel flows in the laminar flux tubes are large enough to deplete the tiny ergodic regions positioned radially behind the laminar flux tubes (Fig. 2). Therefore these regions with locally increasing L_c are not visible neither in n_e nor in T_e for the discharge scenario under discussion.

4. First results from comparative modeling

To analyze the plasma structure and the transport properties in this inherently 3-dimensional magnetic topology the EMC3/EIRENE code was adapted to the requirements of TEXTOR–DED [15]. In order to apply this code to the present discharge, the boundary conditions were set in accordance to the experimental data: the previously determined values for λ_n and λ_T were used and the

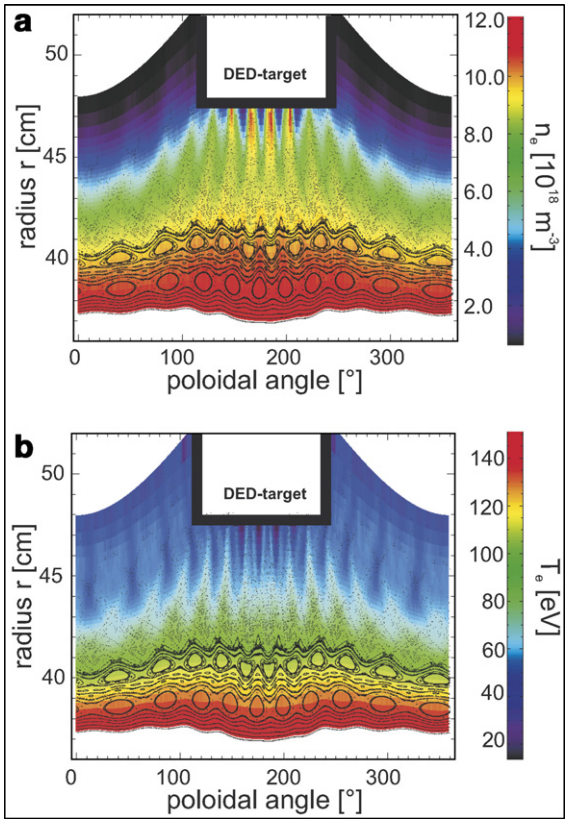

Fig. 3. Distribution of $n_e(\vartheta, r)$ (a) and $T_e(\vartheta, r)$ (b) in the stochastic edge layer at the toroidal position $\varphi = 0°$ modeled with the EMC3/EIRENE code. The structure of the perturbed magnetic field is overlaid as Poincaré plot.

radial transport coefficients were estimated from these values to $D_\perp = 1.4\ \mathrm{m^2\ s^{-1}}$ and $\chi_\perp = 4.1\ \mathrm{m^2\ s^{-1}}$ applying a simple SOL model (see [13, chapter 1]).

The results for $n_e(\vartheta, r)$ and $T_e(\vartheta, r)$ are shown in Fig. 3 in correlation with the Poincaré plot of the perturbed edge: the poloidal modulation of both electron parameters becomes obvious. Localized regions with strongly reduced n_e and T_e values – caused by the *laminar flux tubes* – are interleaved with thin regions with higher n_e and T_e values – the *ergodic regions*. In front of the target, these regions have finger-like structures and they are intersected by private flux regions without direct magnetic connection to the plasma edge and therefore strongly reduced electron parameters.

Associated to the discussion of the experimental results, Fig. 4 shows the direct dependence of the poloidal $n_e(\vartheta)$ and $T_e(\vartheta)$ profiles in the vicinity of a laminar flux tube at the LFS at $r = 0.43$ m. The strong influence of the laminar field lines with short connection to the target is reproduced by this comparative modeling. However, the different behavior of particle and energy transport experimentally detected is not yet visible in these modeling results: inside of the laminar flux tubes, both density and temperature are reduced by a factor of 2 with respect to the unperturbed case. This means that, compared with the experiment, the modeled reduction of the temperature inside the laminar flux tube is too high. An explanation can be given by taking the strong change of the plasma parameters into account. This may lead to a change of the parallel heat conductivity $\kappa_\parallel$ outside the validity of the classical approach which is used in the code equations. This suggests including a kinetic correction for $\kappa_\parallel$ by so-called flux limiters ([13, chapter 26.1]) as it is applied in other fluid codes as well [16]. This work is in progress and the first direct comparisons presented in this paper allow to benchmark and improve the EMC3/EIRENE code.

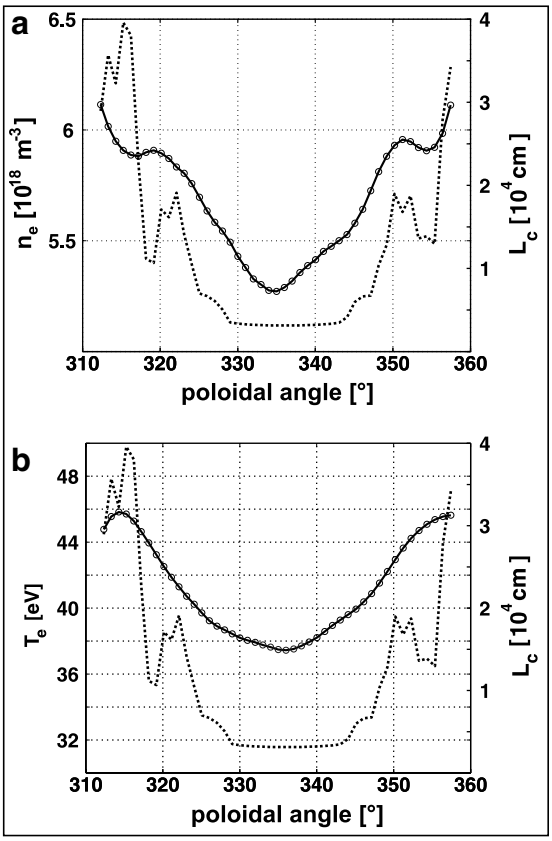

Fig. 4. Comparison of the modeled poloidal profiles $n_e(\vartheta)$ ((a), solid line, circle markers, left axis) and $T_e(\vartheta)$ ((b), solid line, circle markers, left axis) and the connection length $L_c(\vartheta)$ (dashed line, right axis) at $r = 0.43$ m.

5. Conclusion

The poloidal and radial distributions of electron density n_e and temperature T_e are strongly influenced by the magnetic topology of the stochastic edge layer induced by the DED. The detailed comparisons of experimental results with the magnetic topology and the results of 3-dimensional modeling with the EMC3/EIRENE code have shown that laminar flux tubes introduce a domain of convective transport to the wall. Inside these flux tubes, n_e and T_e are strongly reduced owing to a flow of particles and energy to the DED target. In the poloidally adjoining ergodic regions, the values of n_e and T_e are higher due to the stochastic behavior of the ergodic field lines with long connection lengths and enhanced field line diffusion. The competition between both domains determines the transport properties in the perturbed edge layer and the particle and heat load to the DED target. These generic transport properties were successfully reproduced by an initial modeling with the EMC3/EIRENE code. However, the different impact on energy and particle transport indicated by the experimental results is not yet seen in the modeling. As an improvement of the code, a kinetic correction of the parallel heat conductivity is suggested. These findings are of vital importance for the subsequent detailed characterization of the transport mechanisms in this open chaotic system by experimental

data in comparison to the fully 3-dimensional description with the EMC3/EIRENE code.

Acknowledgements

This work has been partially supported by the Sonderforschungsbereich (SFB) 591 of the Deutsche Forschungsgemeinschaft (DFG) and the European Task Force on Plasma–Wall Interaction.

References

[1] R. König et al., Plasma Phys. Control. Fus. 44 (2002) 2365.
[2] S. Masuzaki et al., Nucl. Fus. 42 (2002) 750.
[3] P. Grigull et al., Plasma Phys. Control. Fus. 43 (2001) A175.
[4] T. Evans et al., Nature Phys. 2 (6) (2006) 355.
[5] Ph. Ghendrih et al., Plasma Phys. Control. Fus. 38 (1996) 1653.
[6] K.H. Finken et al., Forschungszentrum Jülich, Series Energy Technology, vol. 45, 2005, ISBN 3-89336-418-8.
[7] M.W. Jakubowski, O. Schmitz, et al., Phys. Rev. Lett. 96 (2006) 035004.
[8] Th. Eich et al., J. Nucl. Mater. 290–293 (2001) 849.
[9] M.Z. Tokar et al., Phys. Plasmas 6 (1999) 2808.
[10] F. Nguyen et al., Nucl. Fus. 37 (1995) 743.
[11] E. Hintz, B. Schweer, et al., Plasma Phys. Control. Fus. 37 (1995) A87.
[12] M. Lehnen et al., J. Nucl. Mater., these Proceedings doi:10.1016/j.jnucmat.2007.01.125.
[13] P.C. Stangeby, The Plasma Boundary of Magnetic Fusion Devices, IOP, 2000.
[14] M. W. Jakubowski et al., J. Nucl. Mater., these Proceedings doi:10.1016/j.jnucmat.2007.01.158.
[15] M. Kobayashi et al., Nucl. Fus. 44 (2004) 6S64.
[16] D.P. Coster et al., J. Nucl. Mater. 337–339 (2005) 366.